Materials Advances

ROYAL SOCIETY OF CHEMISTRY

PAPER

View Article Online
View Journal | View Issue

Cite this: *Mater. Adv.*, 2025, **6**, 6469

Design and synthesis of photoresponsive bent-core liquid crystals exhibiting polar smectic phases

Barbora Jansová, [a] Václav Kozmík, [a] Jiří Svoboda, [a] Martin Krupička,[a] Damian Pociecha, [b] Petr Bečvář, [c] Marcel Bouvet, *[c] Zuzana Böhmová,[d] Vladimíra Novotná [d] and Michal Kohout *[a]

Received 18th April 2025,
Accepted 30th July 2025

DOI: 10.1039/d5ma00379b

rsc.li/materials-advances

Bent-core liquid crystals represent a fascinating class of self-assembling materials. This is due to their unique organized fluidic states – mesophases – that are widely studied for their electro-optical and photonic responses. We designed and synthesized two series of mesogens based on laterally substituted 3-hydroxybenzoic acid, systematically tuning their properties by varying the linking group in both side arms. The mesomorphic behaviour was investigated using polarizing optical microscopy, differential scanning calorimetry (DSC) and X-ray diffraction, revealing the presence of several types of smectic phases. For homologues containing a photoresponsive azo group, we evaluated their light-induced switching in solution as well as in mesophase, under external UV irradiation. We demonstrated that these materials can completely undergo the light-induced switching from a mesophase to an isotropic liquid under *in situ* illumination during X-ray measurements. Unlike previously reported analogues with related structures, the studied compounds exhibited nematic phases with surprisingly narrow temperature range and stable enantiotropic antiferroelectric polar smectic C phases. A transition from a polar SmC to SmC_AP_A phase is also documented.

1. Introduction

Liquid crystals (LCs), unique substances combining anisotropic molecular orientation with a high degree of mobility, have become key examples of modern self-assembling materials.[1] LC materials exhibit a remarkable diversity of self-assembled structures – mesophases, each with its unique symmetry and properties, given by the molecular structure of the building blocks.[2] Bent-core liquid crystals (BCLCs) have emerged as a subject of intense research interest due to their ability to form complex molecular arrangements, leading to the emergence of unique phases such as polar smectic phases. The polar smectic phases of bent-core LCs often exhibit macroscopic chirality despite the lack of an element of chirality in the molecular structure.[3] Moreover, while there is no spontaneous polarization in a classical SmC phase, polarization in the SmCP (where P stands for polar) is perpendicular to the tilt plane and present in each layer due to tight packing of bent-core molecules.[4] The transition from the SmC phase to the SmCP in BCLCs is of particular interest. This transition is driven by subtle changes in the molecular structure and packing, leading to the emergence of long-range polar order. Understanding the factors that govern this transition is crucial for the design and optimization of BCLCs with tailored properties for various applications.

Current research on LCs seeks materials endowed with photoresponsive capability due to their utilization in smart applications.[5,6] From the variety of photoresponsive units, the azo group stands out because of its remarkable chemical and optical stability, and the distinct conditions of photoisomerisation of the thermodynamically more stable *E*-(*trans*-)isomer to the photochemically preferred *Z*-(*cis*-)isomer.[7] These photochromic properties make the azo-based LCs ideal components of numerous molecular devices and functional materials.[8–10] Photoresponsive BCLCs are particularly promising for light-tunable optical gratings, which can be utilized in light steering systems.[11] This is because of large flexoelectric effect typically observed in nematic phases formed by BCLCs.[12] Additionally, optical memory devices have been fabricated using photoresponsive

[a] *Department of Organic Chemistry, University of Chemistry and Technology Prague, Technická 5, CZ-166 28 Prague 6, Czech Republic. E-mail: michal.kohout@vscht.cu*
[b] *Laboratory of Dielectrics and Magnetics, Chemistry Department, Warsaw University, Al. Zwirki i Wigury 101, 02-089 Warsaw, Poland*
[c] *Institut de Chimie Moléculaire de l'Université de Bourgogne, UMR CNRS 6302, Université de Bourgogne, 9 Avenue Alain Savary, Dijon Cedex 21078, France. E-mail: marcel.bouvet@u-bourgogne.fr*
[d] *Institute of Physics, Czech Academy of Sciences, Na Slovance 2, CZ-182 21 Prague 9, Czech Republic*

BCLCs thereby documenting another possible application of these materials.[13] Also in this case, the utilized BCLC exhibited a stable nematic phase, which is in line with the general view of the applicability of bent-core nematogens.[14,15]

Reviews on the chemical structure–mesomorphic properties relationship of BCLCs in general,[16] as well as for their photoresponsive variant,[17] showed that the design of a material with defined properties is a complicated task.[18,19] Therefore, having a broad variety of structures for reference is essential.[20,21] With this knowledge available, the design of advanced structures oriented towards energy conversion and storage,[22] or luminescent systems with potential applications in optics is feasible.[23] In our previous study, we showed that for materials based on 4-chlororesorcinol central core, the nematic phase was stabilized by some linking units in the elongating side arm of the BCLCs.[24] For similar resorcinol-based materials, it was documented that lateral substitution significantly influenced the mesomorphic behaviour.[17] Moreover, elongation of the terminal alkyl chains led to stabilization of the formed mesophases in broad temperature range, eventually leading to the stabilization of complex B_4 and dark conglomerate phases down to room temperature.[25–27]

Here, we introduce a new series of bent-core LCs based on a previously established central unit, namely 3-hydroxybenzoic acid.[28,29] Mesomorphic properties dependence on the lateral substitution with chlorine or fluorine on the central core as well as the character of the linking groups and their orientation while introducing long stabilizing terminal alkyl chains were the focal points. With the aim to tune the mesomorphic properties of the materials, the type of linking unit in the lengthening arm was varied with increasing rigidity from benzoate ester and biphenyl to azo moieties. In the preceding studies on non-photoresponsive materials,[28–31] the preferential formation of a nematic phase was observed for materials with lateral substituent (F, Cl, CH_3) in the position 4 of the central core. It should be noted that the length of terminal alkyl chains was limited to tetradecyl chains ($C_{14}H_{29}$) in all these studies. The hexadecyl terminal chain ($C_{16}H_{33}$) used in this contribution led to significant differences in the mesomorphic behaviour in comparison to the previously described materials.

2. Synthesis

2.1. Synthetic procedure

The synthesis started from 4-chloro-3-methoxybenzoic acid (**1**) and 4-fluoro-3-hydroxybenzoic acid (**2-F**), respectively. The protected central cores (**3-F**, **4-F** and **4-Cl**) were prepared according to known synthetic protocols (Scheme 1).[32–34] In order to study the chemical structure–property relationship in detail, two different types of elongating side arms were prepared following previously reported methods.[25,35,36] While alkoxy phenols **5–8** were prepared *via* alkylation reactions, alkoxy acids **9–11** were synthesized through alkylation of the corresponding esters followed by hydrolysis. The detailed synthetic procedures are provided in the SI.

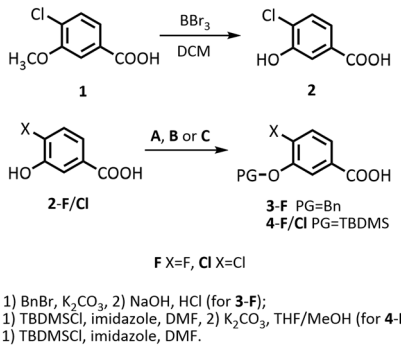

Scheme 1 Synthesis of protected central cores.

The synthesis of the target materials of series **I** and **II** started with *N*,*N*′-dicyclohexylcarbodiimide (DCC)-mediated esterification of the protected central cores with the corresponding elongating side arms in the presence of *N*,*N*-dimethylaminopyridine (DMAP) as a catalyst (Scheme 2). Subsequently, the protecting group was removed with respect to its nature giving rise to intermediates **12-F/Cl-15-F/Cl**, which differ in the lateral substitution and linking units. Depending on the nature of the protecting group, deprotection was performed either by catalytic hydrogenation (benzyl group) or by treatment with fluoride anions (TBDMS group), as described previously.[23] In the final step, the resulting hydroxy esters **12-F/Cl-15-F/Cl** were acylated with the second elongating side arms **9–11** using either acid

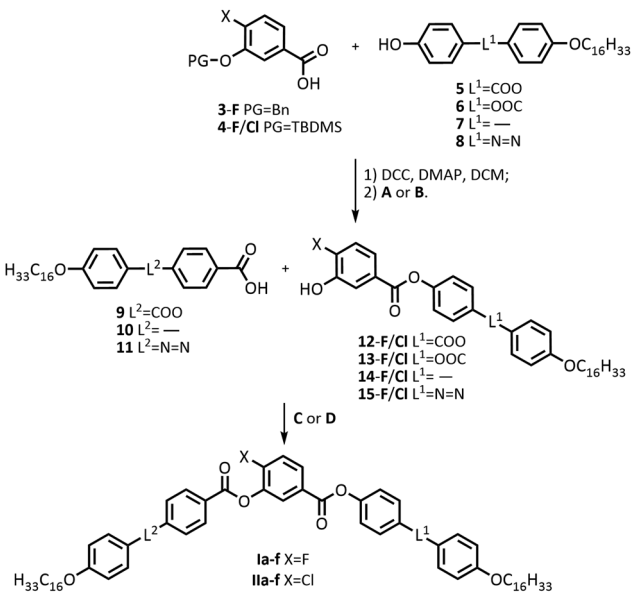

Scheme 2 The synthetic route of the compounds of series **I** and **II**. Final compounds from series **I** and **II** were denoted with additional letters, **a** for L^1 = COO, L^2 = COO, **b** for L^1 = COO, L^2 = —, **c** for L^1 = COO, L^2 = N = N, **d** for L^1 = OOC, L^2 = COO, **e** for L^1 = —, L^2 = COO, **f** for L^1 = N = N, L^2 = COO.

chloride strategy or *N*-ethyl-*N*′-(3-dimethylaminopropyl)carbodiimide (EDC)-mediated esterification.

2.2. Characterisation

The structures of all materials and their intermediates were confirmed by ^{1}H and ^{13}C NMR spectroscopy (Varian Gemini 300 HC and Agilent 400 MR DDR2 instruments). Spectra were measured in deuterated solvents (chloroform and methanol), with residual solvent signals used as internal reference, J values being given in Hz. The purity of the final compounds was confirmed by HPLC analysis. Reactions progress was monitored using TLC on glass plates precoated with silica gel Kiesel 60 GF254 purchased from Merck. Column chromatography was performed using Merck Kiesegel 60 (60–100 μm). The experimental part summarises procedures for the synthesis of intermediates and the target compounds of series **I** and **II**.

2.3. Experimental methods and set-up

Thermal properties of the prepared materials were studied by differential scanning calorimetry (DSC) using a PerkinElmer 7 Pyris calorimeter (PerkinElmer, Shelton, CT, USA). Phase transition temperatures and associated enthalpy changes were established during heating and cooling runs at a rate of 10 K min^{-1}. We calibrated the temperature and enthalpy values on extrapolated onset for melting points of water, indium and zinc. We scaled a small amount of compound 2–5 mg and hermetically sealed in aluminium pans, which was put into the calorimeter chamber. A nitrogen atmosphere was applied during calorimetric measurements.

Phases were identified from observation of textures under a polarizing microscope Eclipse E600Pol (Nikon, Tokyo, Japan). The cells for electro-optical studies were prepared from glasses with ITO transparent electrodes separated by a spacer defining the cell thickness. Studied materials were filled such cells in the isotropic phase (Iso) by capillary action. Another type of cell (one-free-surface sample) was prepared by removing the upper glass during cooling from the isotropic phase. The Linkam LTS E350 heating/cooling stage with TMS 93 temperature programmer (Linkam, Tadworth, UK) was utilized, temperature stabilization reached within ±0.1 K.

A digital oscilloscope Tektronix DPO4034 (Tektronix, Beaverton, OR, USA) was utilized to obtain information about the switching current profile *versus* time. Polarization, P, was determined from the switching current profile. Electric field of triangular modulation at frequency of 50 Hz was applied with magnitude of 20 V μm^{-1}.

The absorption was detected by spectrometer Shimadzu UV-2600 (Shimadzu, Kyoto, Japan). The concentration of the sample in trichlormethan was 0.015 mg ml^{-1}. The cuvette with the measured solution was placed at the distance of 1.5 cm from UV lamp Herolab (Wiesloch, Germany) and illuminated with UV light. The measurements were performed at 365 nm with intensity of 850 μW cm^{-2}. In the polarizing microscope, textures were observed under illumination with an intensive LED lamp UV light (365 nm), source HTLD-4II UV LED (Heigh-LED, ShenZhen, China).

The X-ray scattering measurements were performed to determine the structural properties of studied compounds. For experiments in broad angle range a Bruker GAADS system was used, equipped with microfocus-type X-ray source with Cu anode and dedicated optics to form parallel incident beam, 0.5 mm point-beam collimator and Vantec-2000 area detector. Temperature of the samples, in form of droplets on heated surface, was controlled within 0.1 K with modified Linkam heating stage. Small-angle X-ray diffraction experiments were carried out using Bruker NanoStar (microfocus-type X-ray source with Cu anode and dedicated optics, 3 pinhole beam collimation system and Vantec-2000 area detector). Samples were prepared in thin-walled glass capillaries and their temperature was controlled to within 0.1 K with MRI TCPU_H unit.

Ab initio calculations were performed using Gaussian 03 and molecular structures were visualized with Gaussview 03.[37] Density functional theory (DFT) calculations were employed to optimize the side arms of the molecules using the B3LYP functional with def2-SVP basis set and the RIJCOSX approximation along the def2/J auxiliary basis set. To determine the minimum-energy conformers of the target compounds, (DFT calculations were carried out) in ORCA 4.2.0 software[38–40] using B3LYP functional with the def2-SVP basis set and Grimme's D3 dispersion correction with Becke–Johnson damping (D3BJ). All calculations were performed for isolated single molecules in the gas phase. The results are summarized in the SI.

3. Results and discussion

3.1. Mesomorphic behaviour

Based on the lateral substituent on the central core, the prepared materials were divided into two series: series **I** with lateral fluorine substituent, and series **II** with lateral chlorine substituent. The type of the linking unit in the elongating side arms (L^1 and L^2) changed in a consistent manner in both series. It should be noted that all studied compounds ended symmetrically with long terminal alkyl chains, $C_{16}H_{33}$. The mesomorphic properties as determined from DSC measurements (examples of thermograms are shown in Fig. 1) and optical observations are summarized in Table 1. For all studied materials, the formation of at least one SmCP-type phase was observed. The relatively high transition enthalpies observed at the SmC_AP_A–Iso phase transitions are consistent with the presence of polar order and strong intermolecular interactions, which are typical for polar smectic phases. For fluoro-substituted materials, series **I**, a uniform behaviour with the formation of one smectic mesophase was observed except for **Ic**. We established the character of all mesophases according to the textures and their behaviour in the applied electric field. For compounds **Ia**, **Ib**, **Id** and **If**, we can confirm that the observed SmCP mesophase corresponds to the SmC_AP_A phase. This can be documented by a planar texture of compound **Ia** in the SmC_AP_A phase with fan-shaped structure and characteristic stripes (Fig. 2), which reflect borders between various homochiral domains. Under the applied electric field, transformation to the SmC_SP_F phase takes place and

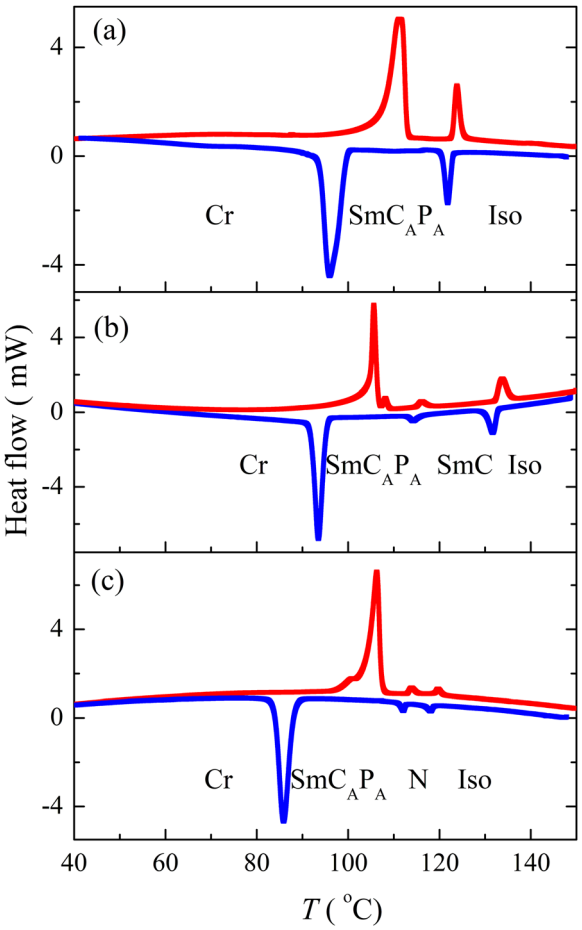

Fig. 1 DSC thermograms taken on the second heating (red) and cooling (blue) for (a) **Ie**, (b) **IIc**, and (c) **IIf**. The intervals of the existence of mesophases are marked in figures within corresponding temperature intervals.

the planar texture shows a change of the extinction position and homochiral domains are visible (Fig. 2(b)).

For **Ic**, there is a sequence of two smectic mesophases. In the upper phase, the planar texture shows a fan-shaped texture, see Fig. 3(a). There is no response to the applied electric field, therefore, it is suggested that this mesophase has a calamitic nature and we can identify it with a SmC phase. On further cooling, the stripes appear in another mesophase, which appeared below the SmC phase, see Fig. 3(b). Contrary to the SmC phase, a lower temperature mesophase exhibits switching under applied electric field. Thus, this mesophase can be identified with the SmC$_A$P$_A$ phase. We can see how the SmC$_A$P$_A$ phase transforms to the SmC$_S$P$_F$ phase during POM observations in Fig. 3(c).

For compound **IIa**, only one mesophase has been detected and identified as SmC$_A$P$_A$ phase due to its polar properties and behaviour under the applied electric field. In regular sandwich cells, the textures showed characteristic fan-shaped features with characteristic transformation in applied field. On the other hand, textures for one-free-surface sample exhibited unusual features in the SmC$_A$P$_A$ phase for several compounds with a direct Iso–SmC$_A$P$_A$ phase transition during the cooling process. There were modulations on a schlieren texture, which are visible predominantly in the vicinity of the isotropic–SmCP phase transition. Fig. 4 shows such a texture in a sample with one-free-surface. Such modulations reflect a specific defect structure existing due to interaction with air on the sample surface.

For **IIb**, an additional phase has been observed below the SmC$_A$P$_A$ phase upon cooling. This phase designated CrX revealed a crystalline character, as has been proven during XRD studies. In the compound **IIc**, we have detected two smectic C phases of similar character observed for **Ic**. According to the

Table 1 Data from DSC thermographs recorded during the second cooling/heating run at a rate of 10 K min^{-1}. Melting points, m.p., phase transition temperatures, T_{tr}, and crystallisation temperatures, T_{cr}, and the temperatures of the isotropic (Iso)-mesophase transformation, T_{iso}, are in °C and corresponding enthalpy changes, ΔH, are given in kJ mol^{-1} in square brackets

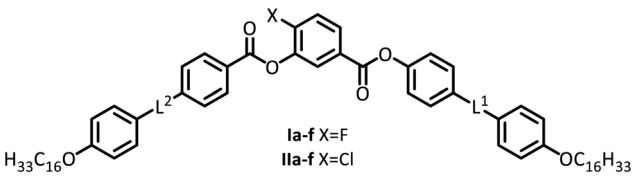

		Linking units								
	X	L^2	L^1	m.p. [ΔH]	T_{cr} [ΔH]	M$_2$	T_{tr} [ΔH]	M$_1$	T_{iso} [ΔH]	Iso
Ia	F	COO	COO	111 [+52.0]	108 [−59.6]			SmC$_A$P$_A$	133 [−8.96]	•
Ib	F	—	COO	104 [+92.6]	86 [−76.1]			SmC$_A$P$_A$	131 [−14.6]	•
Ic	F	N = N	COO	123 [+78.7]	101 [−31.6]	SmC$_A$P$_A$	123 [−2.16]	SmC	148 [−9.4]	•
Id	F	COO	OOC	112 [+63.7]	91 [−524.4]			SmC$_A$P$_A$	99 [−14.4]	•
Ie	F	COO	—	106 [+46.3]	99 [−48.7]			SmC$_A$P$_A$	120 [−12.8]	•
If	F	COO	N = N	107 [+47.1]	100 [−48.0]			SmC$_A$P$_A$	123 [−7.83]	•
IIa	Cl	COO	COO	105 [+124.7]	97 [−99.0]			SmC$_A$P$_A$	121 [−5.30]	•
IIb	Cl	—	COO	106 [+47.2]	105 [−48.3]	CrX	114 [−1.26]	SmC$_A$P$_A$	128 [−6.02]	•
IIc	Cl	N = N	COO	105 [+41.7]	95 [−46.3]	SmC$_A$P$_A$	116 [−2.93]	SmC	133 [−8.31]	•
IId	Cl	COO	OOC	121 [+97.5]	76 [−64.2]	SmC$_A$P$_A$	104 [−2.87]	N	109 [−1.58]	•
IIe	Cl	COO	—	94 [+37.7]	72 [−26.6]			SmC	112 [−8.78]	•
IIf	Cl	COO	N = N	104 [+69.5]	88 [−67.8]	SmC$_A$P$_A$	113 [−1.31]	N	118 [−1.99]	•

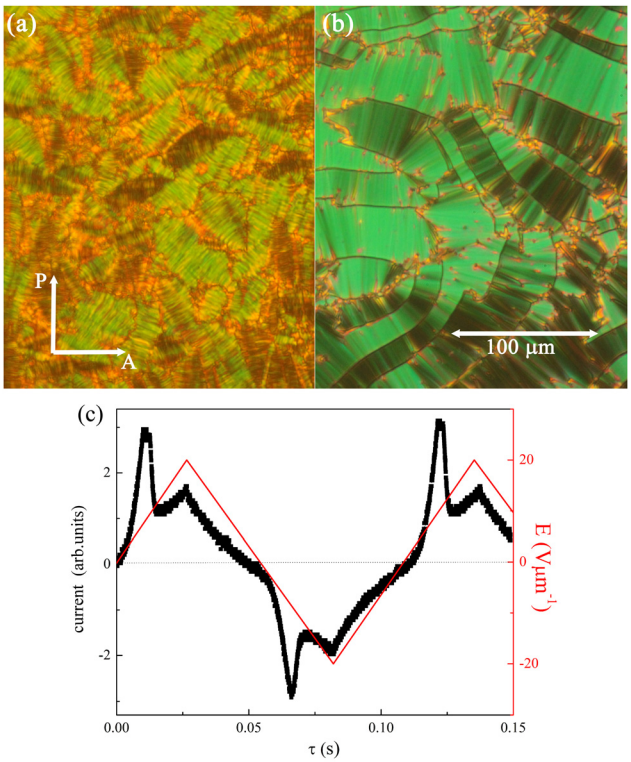

Fig. 2 Planar texture of **Ia** in the SmC_AP_A phase at T = 120 °C (a) before the application of the electric field, and (b) under the field of about 15 V μm^{-1}. The orientation of polarizer (P) and analyser (A) is marked. (c) Switching current profile in the SmC_AP_A phase at T = 100 °C.

textural features under the applied electric field, we can establish the SmC–SmC_AP_A phase sequence for the compound **IIc**. Smectic character of both mesophases has been confirmed by XRD measurements, see later.

A distinct phase sequence has been found for **IId** and **IIf**. The initial liquid crystalline phase formed on cooling from the isotropic liquid is a nematic phase (N), see Fig. 5(a) for **IIf**. On further cooling, the N phase turns to the SmC_AP_A phase (Fig. 5(b)), whose texture under the electric field can be transformed to the SmC_SP_F phase (Fig. 5(c)). The effect of the applied field can be documented by the presence of the switching current (Fig. 5 for **IIf**). For the compound **IIe** we have detected only one mesophase, namely a non-switchable smectic C phase. Thus, we can conclude that there is the SmC phase.

Generally, the change of fluorine to chlorine as the lateral substituent on the central core led to a decrease of transition temperatures. This effect is more pronounced for materials **IId-f** that exhibited crystallization well below 100 °C. Moreover, a significant difference in the mesomorphic behaviour was observed for these compounds in comparison to materials **Id–f**. This is documented by the emergence of the nematic phase for compounds **IId** and **IIf**, and the loss of the polar arrangement of the mesophase of compound **IIe**. This behaviour could be ascribed to the steric effect of the chlorine atom, which leads to conformational change of the more flexible side wing adjacent to chlorine in the case of materials **IId–f** (see below).

Another structural feature influencing the character of the mesomorphic behaviour of the new materials is the orientation of ester linkages. In this case, reduced phase transition temperatures were observed on the reversal of the orientation of the ester linkage in materials **Ia** *vs.* **Id** and **IIa** *vs.* **IId**. Such a trend was previously observed also for the derivatives of 3-hydroxybenzoic acid with shorter terminal alkyl chains.[28,29]

3.2. X-ray diffraction measurements and *ab initio* calculations

The XRD measurements provided detailed structural insight into observed smectic mesophases. The lamellar character of these mesophases has been confirmed by the characteristic profiles of XRD intensity *versus* scattering angle (Fig. 6). In the small-angle region of the XRD patterns a series of sharp commensurate signals was observed corresponding to long-range regular arrangement of smectic layers. On the other hand, a broad diffuse maximum that has been detected for

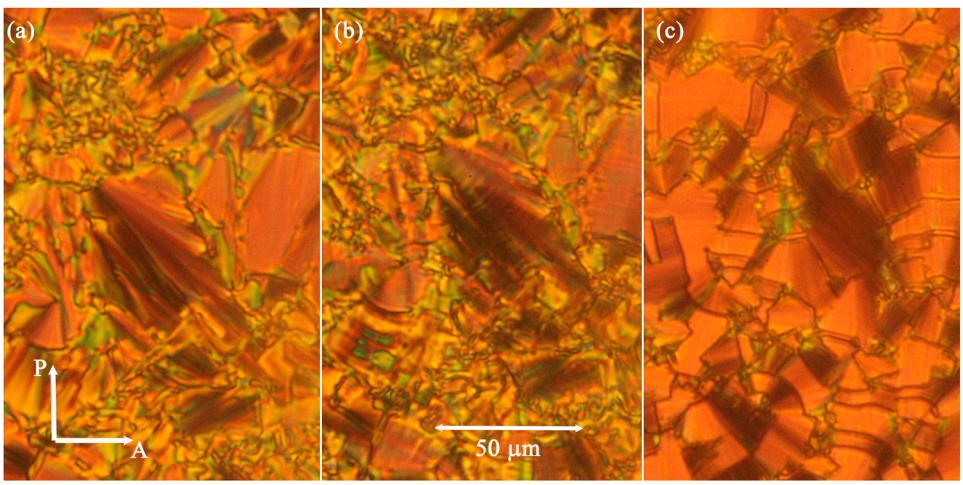

Fig. 3 Planar texture of **Ic** taken in (a) the SmC phase at T = 140 °C, (b) in the SmC_AP_A phase at T = 120 °C, and (c) in the SmC_AP_A phase under the applied field at the same temperature T = 120 °C. The orientation of the polarizer (P) and the analyser (A) are marked, being common for all photos.

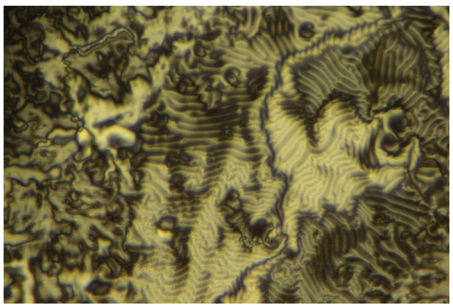

Fig. 4 Schlieren texture observed in a sample with one-free-surface of **IIa** in the SmCP phase at T = 120 °C. Periodic modulations are observed only in close vicinity of the Iso–SmCP phase transition. The width of the figure corresponds to about 250 μm.

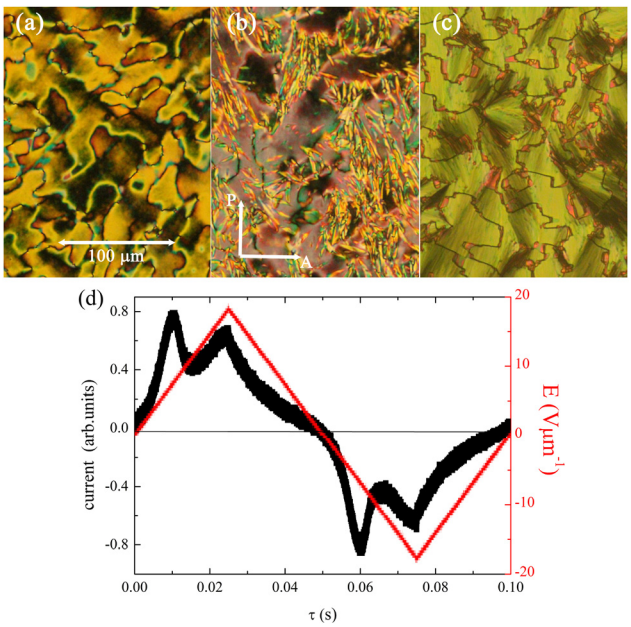

Fig. 5 Planar texture of **IIf** taken in (a) the nematic phase at T = 115 °C, (b) at the N–SmC$_A$P$_A$ phase transition at T = 113 °C, and (c) the SmC$_A$P$_A$ phase at T = 110 °C under the applied field of 15 V μm^{-1}. Polarizer (P) and analyser (A) are in a crossed position during all observations, in the orientation marked in (b) photo. (c) Switching current profile in the SmC$_A$P$_A$ phase at T = 108 °C.

all compounds in the wide-angle region of the patterns evidenced the lack of the long-range in-plane order of molecules, thus confirmed liquid-like type smectic phase identification. In all cases position of the high angle signal corresponded to ~4.5 Å, reflecting an average distance between bent-core molecules within the smectic layers. In order to precisely determine temperature dependence of the smectic layer thickness, $d(T)$, small angle diffraction experiments were performed. It was found that for compound **Ib** layer spacing monotonically increases on cooling in the SmC$_A$P$_A$ phase (Fig. 7). For compounds with the SmC–SmC$_A$P$_A$ phase sequence the layer spacing showed non-monotonic behaviour (Fig. 8 and Fig. S3), namely it slightly decreased on cooling in SmC phase, while in SmC$_A$P$_A$ phase an increase of d was observed, similarly as for

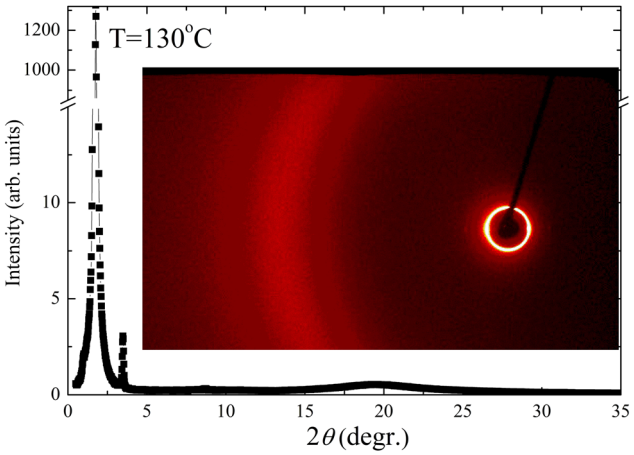

Fig. 6 The X-ray intensity profile *versus* the scattering angle, θ, obtained by integration of corresponding 2D pattern (inset) recorded for compound **Ia** at T = 130 °C, in the SmC$_A$P$_A$ phase.

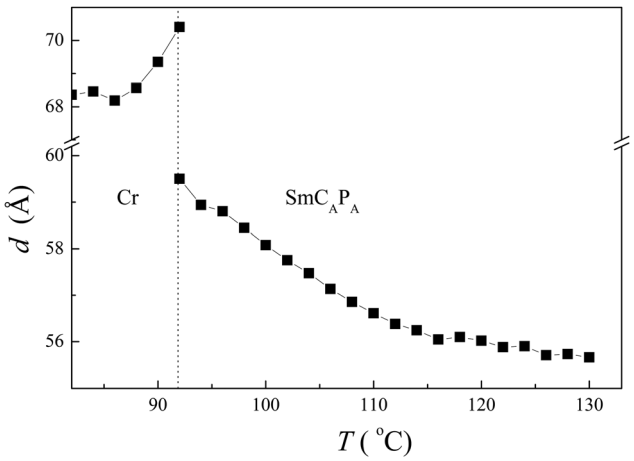

Fig. 7 Temperature dependence of the layer spacing, d, for **Ib**.

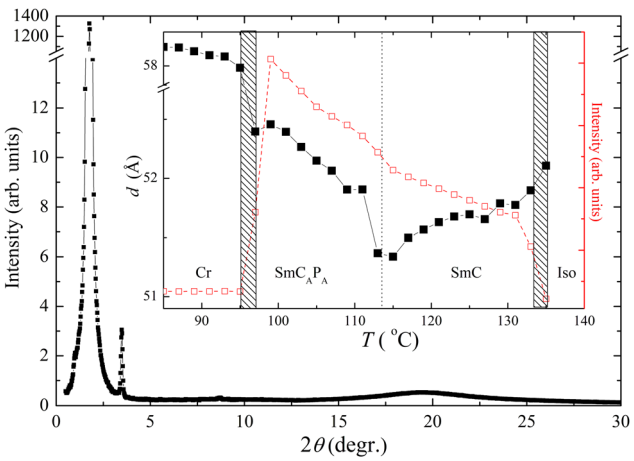

Fig. 8 The X-ray intensity profile *versus* the scattering angle, θ, recorded for compound **IIc** at the T = 130 °C. In the inset, the temperature dependence of the layer spacing, d, and corresponding intensity of the XRD signal. The phase interval is indicated. A coexistence of neighbouring phase is hatched by a pattern.

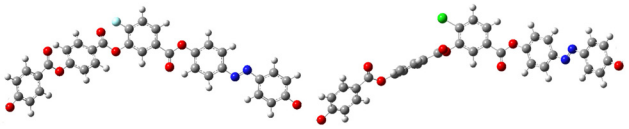

Fig. 9 Conformers with minimum energy obtained by *ab initio* calculations for structures of materials **If** and **IIf**. Full pictures of the calculated materials are depicted in SI, Fig. S6 and S7.

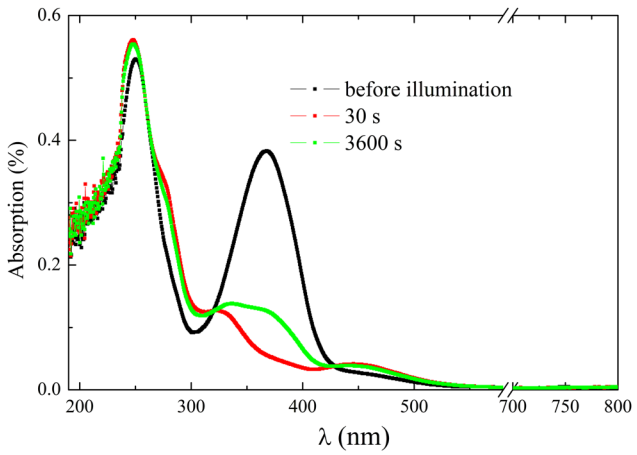

Fig. 10 UV/Vis spectra for **IIc** (in a chloroform solution in concentration 0.015 mg ml^{-1}), measured in darkness before (black), and after the illumination with UV-light (365 nm) for 30 seconds (red curve). Rather slow relaxation (after 1 hour) is also documented (green curve).

compounds forming exclusively SmC_AP_A. We can speculate that in the SmC phase the tilt of molecules increases, which leads to slight decrease of the layer thickness. Slight growth of the layer spacing on the cooling in a SmCP phase can be attributed to considerable increase of orientational order of molecules due to appearance of polar order and a stretching of terminal chains.

The above commented difference in the mesomorphic behaviour of materials **Id-f** in comparison to materials **IId-f** was studied using two selected representatives (**If** and **IIf**). The conformers with minimum energy for fluoro-substituted material **If** exhibited the angle between the elongating side arms of 128°, which is close to the optimum value of 120° for the bending angle in bent-core liquid crystals.[41] Slightly larger value of the bending angle (131°) was found for the chloro-substituted homologue **IIf** (Fig. 9). This could be caused by the size of the chlorine atom and mutual repulsion of the electron shells of chlorine and oxygen from the carbonyl group. This repulsion is more pronounced than in case of chlorine (dihedral angle with C═O, −98.4°) than fluorine (dihedral angle with C═O, 60.0°) as the lateral substituent. These differences give rise to the change in the molecular structure and, consequently, to alteration in the molecular packing and different mesomorphic behaviour.

3.3. Photoresponsive properties

The azobenzene unit present in the structure of four studied compounds (**Ic**, **If**, **IIc** and **IIf**) renders these materials photoresponsive. The ability of facile *E*-to-*Z* isomerisation of the azo group in bent-core liquid crystals has already been documented in several studies and reviews.[11,17,24] To confirm the photoresponsive behaviour of the new materials, we first performed a UV-Vis study in solution (chloroform as the solvent). As expected, the initial photostationary state was composed predominantly of the more thermodynamically stable *E*-isomer having the absorption maximum at about 360 nm. On illumination of **IIc** with UV light of this wavelength, the absorption band diminished (within 30 s) while the absorption maximum corresponding to the *Z*-isomer (approx. 460 nm) increased documenting the photostationary state composed mainly of the *Z*-isomer (Fig. 10). It takes at least several hours for recovery to the *E*-isomer.

In the next stage, we decided to illuminate the sample with external light under the microscope. As the glass absorbs the UV light, we prepared a sample with one-free-surface, where the compound is not covered by a glass slide, and it is illuminated during the POM observations. The schlieren texture underwent a fast change under the illumination, and the sample is quickly transformed to the isotropic phase. The isotropic phase is seen

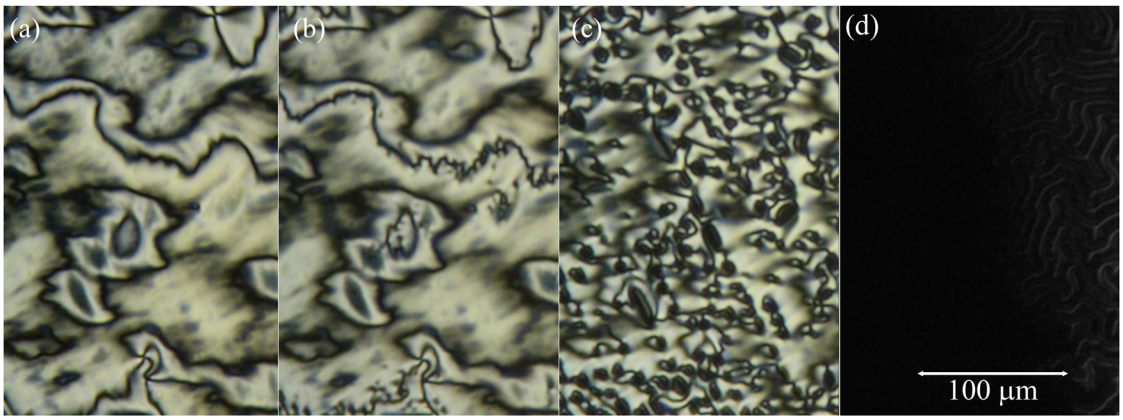

Fig. 11 Textures from the polarized microscope observed for **If** compound (SmC_AP_A phase) (a) before the illumination; (b), (c) and (d) are photos of the same textural part after illumination with an intensive LED lamp (365 nm) for 5 s, 10 s and 20 s, respectively.

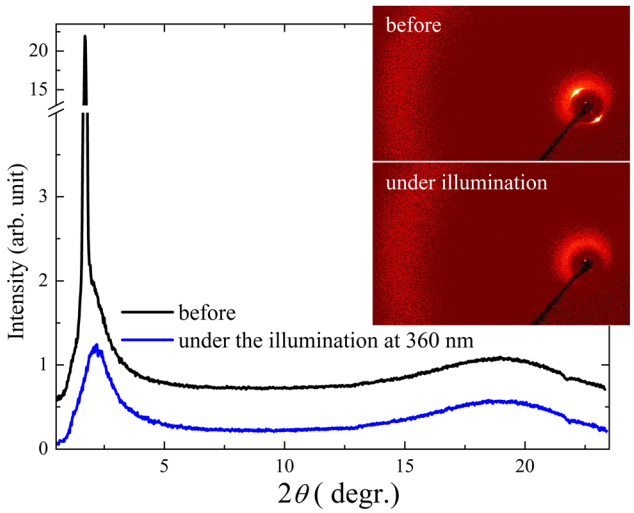

Fig. 12 The X-ray intensity profile *versus* the scattering angle for **Ic** at T = 138 °C before (black curve) and under illumination at 360 nm (blue curve). In the inset there are corresponding 2D patterns before (upper photo) and under the illumination.

in the form of black seeds within the schlieren texture. In Fig. 11 for compound **If**, one can see these seeds of Iso growing under the illumination. After 12 seconds, the compound is completely in the isotropic phase. When switching off the illumination, the texture is reconstructed in 12–18 seconds.

To prove the photoinduced transition to the isotropic phase, we have performed XRD measurements under the illumination. We prepared the sample of **Ic** in the form of a thin film and recorded XRD before and under the illumination with UV light. Prior to irradiation, a sharp peak corresponding to the lamellar structure of the SmCP phase was detected at small angles. Under illumination with UV light of 360 nm, the narrow diffraction peak was gradually replaced with a diffused one, which evidenced the transformation from the lamellar to non-ordered, liquid phase (Fig. 12).

4. Discussion and comparison with similar molecular structures

Previously, several materials with a related structure have been presented, typically differing in the length of the terminal alkyl chains. Nevertheless, no systematic research has been done concerning the effect of the linking group *versus* the length of terminal chains. Therefore, we summarize the available information and compare the previously reported compounds with the materials studied in this contribution (Table 2). Five compounds studied here can be directly compared with previously studied homologues differing in the length of the terminal chain, namely with alkyl $C_{14}H_{29}$. The comparison shows that the elongation of terminal alkyl chains (from $C_{14}H_{29}$ to $C_{16}H_{33}$) in the new materials leads to the stabilization of the smectic arrangement. It is particularly significant for materials with one ester linkage reversed. Materials **Id/F** and **Id/Cl** studied in the previous article[13] exhibited the sequence of a monotropic nematic and unspecified B_X (banana) phase. In this study, materials **Id** and **IId** reveal a SmC_AP_A phase and a sequence of a nematic and SmC_AP_A phases, respectively. Also in this case, the mesomorphic behaviour was monotropic. This means that the elongation of the terminal alkyl chain led to the destabilization of the mesomorphic behaviour, which for the material **Id** resulted in the diminishing of the nematic phase and the formation of the monotropic SmC_AP_A phase only. For material **IId**, the sequence of the nematic and SmC_AP_A phases was preserved, however, the nematic phase was significantly less stable.

Narrow temperature interval of the nematic phase and preference of the smectic arrangement are also significant in

Table 2 Comparison of selected materials studied in this contribution (upper part of the table) with similar compounds described in literature (corresponding references are in square brackets), the designation of compounds is the same as in the original articles. Melting points, m.p., phase transition temperatures, T_{tr}, and crystallisation temperature, T_{cr}, are given in °C

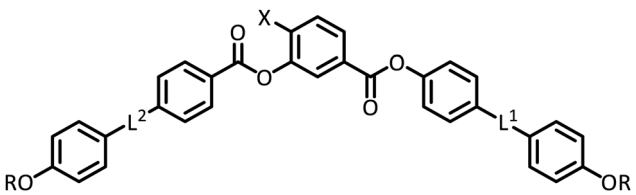

	X	L^2	L^1	R	M.p.	T_{cr}	M_2	T_{tr}	M_1	T_{iso}	Iso
Ia	F	COO	COO	$C_{16}H_{33}$	111	108			SmC_AP_A	133	•
Ic	F	NN=	COO	$C_{16}H_{33}$	123	101	SmC_AP_A	123	SmC	148	•
Id	F	COO	OOC	$C_{16}H_{33}$	112	91			SmC_AP_A	99	•
IIa	Cl	COO	COO	$C_{16}H_{33}$	105	97			SmC_AP_A	121	•
IId	Cl	COO	OOC	$C_{16}H_{33}$	121	76	SmC_AP_A	104	N	109	•
IIId/F	F	COO	COO	$C_{14}H_{29}$	121	115	CrX	122	SmC_AP_A	136	• [12]
SV775	F	N = N	COO	C_8H_{17}	124	105	SmX	110	N	128	• [11]
Id/F	F	COO	OOC	$C_{14}H_{29}$	115	100	B_X	106	N	113	• [13]
IIId/Cl	Cl	COO	COO	$C_{14}H_{29}$	113	102	CrX	112	SmC_AP_A	126	• [12]
Id/Cl	Cl	COO	OOC	$C_{14}H_{29}$	120	80	B_X	93	N	109	• [13]

materials with the azo group in the molecular structure. This can be documented on a pair of photoresponsive materials, namely **Ic** studied here and previously reported **SV775** possessing the octyl terminal alkyl chains.[11] While the previously described **SV775** showed a sequence of enantiotropic nematic and non-specified smectic phase, the extension of the terminal alkyl chains in **Ic** led to the replacement of the nematic phase by a SmC phase and the formation of the fully switchable SmC_AP_A phase.

Similar materials with the uniform orientation of ester linkages (compounds **IIId/F** and **IIId/Cl** studied in ref. 12) exhibited the formation of a SmC_AP_A phase followed by a crystal-crystal transition. The materials studied here, **Ia** and **IIa**, with uniform orientation of ester linkages exhibited exclusively a SmC_AP_A phase. In comparison to the previously studied compounds, the phase transition temperatures were diminished. In another work, we studied an analogue of **SV775** with additional lateral substitution with fluorine adjacent to the azo group.[42] This structural tuning resulted in formation of a monotropic nematic phase only. It should be noted that bent-core liquid crystals based on 4-chlororesorcinol as the central core also typically form nematic phases or a sequence of a nematic phase and polar smectic phase. This is due to the increase in bending angle caused by the presence of the chlorine atom.[41] However, as the terminal alkyl chains are stretched, the smectic arrangement also predominates in these resorcinol-based compounds, eventually leading to complex arrangements such as the B4 phase or B6 phase.[15] These complex chiral mesophases are then promoted by lateral substitution in the outer phenyl rings of the bent core material and long terminal alkyl chains.[17]

5. Conclusion

In the present paper we have focused on the effect of the linkage group type and orientation for long terminal alkyl chains-based materials. It can be concluded that all but one of the azo-containing materials studied in this work exhibit an enantiotropic SmC_AP_A phase. This behaviour is most likely ensured by the long terminal alkyl chains, which strongly stabilise the smectic arrangement. The overall bent shape of the compounds then induces the polar behaviour. Chlorine as a bulkier lateral substituent leads to a looser packing of the molecules resulting in a sequence of N–SmC_AP_A phases, SmC–SmC_AP_A phases, or SmC phase only (compound **IIe**). We have also documented that the studied materials readily respond to illumination with UV light, not only in solution but also in the mesophase. The phase transition upon illumination was confirmed by X-ray intensity profile study, which clearly showed the transition from SmC_AP_A phase to isotropic liquid. The combined response to electric field and light allows the use of this class of compounds in the construction of various devices such as non-binary logic circuits and optical memories. Moreover, some of the materials presented here have recently been utilized as photoactive dielectric layers for novel gas sensors.[43]

Author contributions

B. J.: investigation, writing – original draft, visualization; V. K.: investigation; J. S.: investigation, supervision; M. K.: formal analysis; D. P.: investigation, formal analysis, writing – review and editing; P. B.: investigation; M. B.: funding acquisition, supervision, writing – review and editing; Z. B.: investigation; V. N.: investigation, formal analysis, resources, writing – original draft; M. K.*: conceptualization, resources, funding acquisition, supervision, methodology, writing – review and editing.

Conflicts of interest

The authors declare no conflict of interest.

Data availability

The data supporting this article have been included as part of the SI.

Supplementary information comprising the details on the synthesis of target materials, their characterization, and additional data on mesomorphic properties of the target materials is available. See DOI: **https://doi.org/10.1039/d5ma00379b**

Acknowledgements

The authors acknowledge computational resources provided by e-INFRA CZ project (ID:90254), supported by the Ministry of Education, Youth and Sports of the Czech Republic. P. B. thanks the MESRI for his PhD grant. The Ministry of Education, Youth and Sports of the Czech Republic and the MEAE and MESRI in France are acknowledged for the bilateral Partenariat Hubert Curien between Czech Republic and France (project PHC-Barrande 49226PA) and for a PhD grant (B. J.). The authors gratefully thank Véronique Debord-Lazaro from the French Institute in Prague for her precious help.

References

1 C. Tschierske, *Angew. Chem., Int. Ed.*, 2013, **52**, 8828–8878.
2 P. J. C. John, W. Goodbye, T. Kato, C. Tschierske, H. Gleeson and P. Raynes, *Handbook of Liquid Crystals*, Wiley-VCH, Weinheim, 2014.
3 T. Niori, T. Sekine, J. Watanabe, T. Furukawa and H. Takezoe, *J. Mater. Chem.*, 1996, **6**, 1231–1233.
4 D. R. Link, G. Natale, R. Shao, J. E. Maclennan, N. A. Clark, E. Körblova and D. M. Walba, *Science*, 1997, **278**, 1924–1927.
5 H. K. Bisoyi and Q. Li, *Chem. Rev.*, 2016, **116**, 15089–15166.
6 L. Wang and Q. Li, *Chem. Soc. Rev.*, 2018, **47**, 1044–1097.
7 H. M. D. Bandara and S. C. Burdette, *Chem. Soc. Rev.*, 2012, **41**, 1809–1825.
8 C.-U. Bang, A. Shishido and T. Ikeda, *Macromol. Rapid Commun.*, 2007, **28**, 1040–1044.
9 V. Ferri, M. Elbing, G. Pace, M. D. Dickey, M. Zharnikov, P. Samorì, M. Mayor and M. A. Rampi, *Angew. Chem., Int. Ed.*, 2008, **47**, 3407.

10 Y. Norikane and N. Tamaoki, *Org. Lett.*, 2004, **6**, 2595–2598.
11 H. Jing, M. Xu, Y. Xiang, E. Wang, D. Liu, A. Poryvai, M. Kohout, N. Éber and Á. Buka, *Adv. Opt. Mater.*, 2019, **7**, 1801790.
12 J. Harden, B. Mbanga, N. Éber, K. Fodor-Csorba, S. Sprunt, J. T. Gleeson and A. Jakli, *Phys. Rev. Lett.*, 2006, **97**, 157802.
13 S. Shruthi, M. Smahel, M. Kohout, G. Shanker and G. Hegde, *J. Mol. Liq.*, 2021, **339**, 116744.
14 A. Jákli, *Liq. Cryst. Rev.*, 2013, **1**, 65–82.
15 M. Alaasar, M. Prehm and C. Tschierske, *Liq. Cryst.*, 2013, **40**, 656–668.
16 R. A. Reddy and C. Tschierske, *J. Mater. Chem.*, 2006, **16**, 907–961.
17 M. Alaasar, *Liq. Cryst.*, 2016, **43**, 2208–2243.
18 J. Liebsch, R. Strachan, S. Suthaharan, I. Dominguez-Candela, C. Auria-Soro, A. San-Millan, R. Walker, B. Chilukuri, M. Blanca Ros and A. Martinez-Felipe, *J. Mol. Liq.*, 2024, **399**, 124371.
19 M. Poppe, M. Alaasar, A. Lehmann, S. Poppe, M.-G. Tamba, M. Kurachkina, A. Eremin, M. Nagaraj, J. K. Vij, X. Cai, F. Liu and C. Tschierske, *J. Mater. Chem. C*, 2020, **8**, 3316–3336.
20 M. Alaasar, S. Poppe, C. Kerzig, C. Klopp, A. Eremin and C. Tschierske, *J. Mater. Chem. C*, 2017, **5**, 8454–8468.
21 G. Mohiuddin, N. Begum, N. V. S. Rao, B. K. Debbarma, R. Nandi, A. Saeed and N. Haq, *J. Mol. Struct.*, 2025, **1339**, 142440.
22 I. Dominguez-Candela, I. Zulkhairi, I. Pintre, N. F. K. Aripin, J. Lora-Garcia, V. Fombuena, M. B. Ros and A. Martinez-Felipe, *J. Mater. Chem. C*, 2022, **10**, 18200–18212.
23 M. Martínez-Abadía, S. Varghese, J. Gierschner, R. Giménez and M. B. Ros, *J. Mater. Chem. C*, 2022, **10**, 12012–12021.
24 M. Šmahel, A. Poryvai, Y. Xiang, D. Pociecha, T. Troha, V. Novotna, J. Svoboda and M. Kohout, *J. Mol. Liq.*, 2020, **306**, 112743.
25 M. Alaasar, M. Prehm, K. May, A. Eremin and C. Tschierske, *Adv. Funct. Mater.*, 2014, **24**, 1703–1717.
26 M. Alaasar, M. Prehm and C. Tschierske, *Chem. Commun.*, 2013, **49**, 11062–11064.
27 M. Alaasar, M. Prehm and C. Tschierske, *Chem. – Eur. J.*, 2016, **22**, 6583–6597.
28 M. Kohout, V. Kozmík, M. Slabochová, J. Tůma, J. Svoboda, V. Novotná and D. Pociecha, *Liq. Cryst.*, 2015, **42**, 87–103.
29 J. Tůma, M. Kohout, J. Svoboda, V. Novotná and D. Pociecha, *Liq. Cryst.*, 2016, **43**, 547–563.
30 J. Tůma, M. Kohout, J. Svoboda, V. Novotná and D. Pociecha, *Liq. Cryst.*, 2016, **43**, 1889–1900.
31 L. Pallová, V. Kozmík, M. Kohout, J. Svoboda, V. Novotná and D. Pociecha, *Liq. Cryst.*, 2017, **44**, 1306–1315.
32 E. L. Elliott, S. M. Bushell, M. Cavero, B. Tolan and T. R. Kelly, *Org. Lett.*, 2005, **7**, 2449–2451.
33 M. Bone, M. Bradshaw, L. Chan, D. Coates, J. Constant, P. Gemmell, G. Gray, D. Lacey and K. Toyne, *Mol. Cryst. Liq. Cryst. Incorporat. Nonlinear Opt.*, 1988, **164**, 117–134.
34 F. Claudi, G. Giorgioni, A. Di Stefano, M. P. Abbracchio, A. M. Paoletti and W. Balduini, *J. Med. Chem.*, 1992, **35**, 4408–4414.
35 J. M. El Khoury, X. Zhou, L. Qu, L. Dai, A. Urbas and Q. Li, *Chem. Commun.*, 2009, 2109–2111.
36 M. Kohout, J. Svoboda, V. Novotná, D. Pociecha, M. Glogarová and E. Gorecka, *J. Mater. Chem.*, 2009, **19**, 3153–3160.
37 M. J. Frisch, G. W. Trucks, H. B. Schlegel, G. E. Scuseria, M. A. Robb, J. R. Cheeseman, G. Scalmani, V. Barone, G. A. Petersson, H. Nakatsuji, X. Li, M. Caricato, A. V. Marenich, J. Bloino, B. G. Janesko, R. Gomperts, B. Mennucci, H. P. Hratchian, J. V. Ortiz, A. F. Izmaylov, J. L. Sonnenberg, D. Williams, F. Ding, F. Lipparini, F. Egidi, J. Goings, B. Peng, A. Petrone, T. Henderson, D. Ranasinghe, V. G. Zakrzewski, J. Gao, N. Rega, G. Zheng, W. Liang, M. Hada, M. Ehara, K. Toyota, R. Fukuda, J. Hasegawa, M. Ishida, T. Nakajima, Y. Honda, O. Kitao, H. Nakai, T. Vreven, K. Throssell, J. A. Montgomery Jr., J. E. Peralta, F. Ogliaro, M. J. Bearpark, J. J. Heyd, E. N. Brothers, K. N. Kudin, V. N. Staroverov, T. A. Keith, R. Kobayashi, J. Normand, K. Raghavachari, A. P. Rendell, J. C. Burant, S. S. Iyengar, J. Tomasi, M. Cossi, J. M. Millam, M. Klene, C. Adamo, R. Cammi, J. W. Ochterski, R. L. Martin, K. Morokuma, O. Farkas, J. B. Foresman and D. J. Fox, *Gaussian 16, Revision C.01*, Gaussian, Inc., Wallingford CT, 2016.
38 F. Neese, *Wiley Interdiscip. Rev.: Comput. Mol. Sci.*, 2012, **2**, 73–78.
39 F. Neese, *Wiley Interdiscip. Rev.: Comput. Mol. Sci.*, 2018, **8**, e1327.
40 F. Neese, F. Wennmohs, U. Becker and C. Riplinger, *J. Chem. Phys.*, 2020, **152**, 224108.
41 W. Weissflog, H. Nádasi, U. Dunemann, G. Pelzl, S. Diele, A. Eremin and H. Kresse, *J. Mater. Chem.*, 2001, **11**, 2748–2758.
42 D. Jágerová, M. Šmahel, A. Poryvai, J. Macháček, V. Novotná and M. Kohout, *Crystals*, 2021, **11**, 1265.
43 B. Jansová, M. Sujithkumar Ganesh, M. Šmahel, E. Lesniewska, M. Kohout and M. Bouvet, *Adv. Sensor Res.*, 2025, **4**, e00026.